Cellulose (2018) 25:23–36
https://doi.org/10.1007/s10570-017-1549-6

ORIGINAL PAPER

Structural factors affecting ^{13}C NMR chemical shifts of cellulose: a computational study

Hui Yang · Tuo Wang · Daniel Oehme · Loukas Petridis · Mei Hong · James D. Kubicki

Received: 31 May 2017 / Accepted: 30 October 2017 / Published online: 2 November 2017

Abstract The doublet C4 peaks at ~ 85 and ~ 89 ppm in solid-state ^{13}C NMR spectra of native cellulose have been attributed to signals of C4 atoms on the surface (solvent-exposed) and in the interior of microfibrils, designated as sC4 and iC4, respectively. The relative intensity ratios of sC4 and iC4 observed in NMR spectra of cellulose have been used to estimate the degree of crystallinity of cellulose and the number of glucan chains in cellulose microfibrils. However, the molecular structures of cellulose responsible for the specific surface and interior C4 peaks have not been positively confirmed. Using density functional theory (DFT) methods and structures produced from classical molecular dynamics simulations, we investigated how the following four factors affect ^{13}C NMR chemical shifts in cellulose: conformations of exocyclic groups at C6 (*tg*, *gt* and *gg*), H_2O molecules H-bonded on the surface of the microfibril, glycosidic bond angles (Φ, Ψ) and the distances between H4 and HO3 atoms. We focus on changes in the $\delta^{13}C4$ value because it is the most significant observable for the same C atom within the cellulose structure. DFT results indicate that different conformations of the exocyclic groups at C6 have the greatest influence on $\delta^{13}C4$ peak separation, while the other three factors have secondary effects that increase the spread of the calculated C4 interior and surface peaks.

Electronic supplementary material The online version of this article (https://doi.org/10.1007/s10570-017-1549-6) contains supplementary material, which is available to authorized users.

H. Yang
Department of Biology, Pennsylvania State University, University Park, PA, USA

T. Wang · M. Hong
Department of Chemistry, Massachusetts Institute of Technology, Cambridge, MA, USA

D. Oehme
ARC Centre of Excellence in Plant Cell Walls, School of Biosciences, University of Melbourne, Melbourne, VIC, Australia

L. Petridis
Center for Molecular Biophysics, Oak Ridge National Laboratory, Oak Ridge, TN, USA

J. D. Kubicki (✉)
Department of Geological Sciences, University of Texas at El Paso, El Paso, TX, USA
e-mail: jdkubicki@utep.edu

Present Address:
T. Wang
Department of Chemistry, Louisiana State University, Baton Rouge, LA, USA

Keywords Cellulose · NMR · DFT · MD simulation · Microfibril

Introduction

Plant cell walls (PCWs) are the most abundant renewable source of carbohydrates on Earth (Duchesne and Larson 1989). PCWs are sophisticated assemblies of cellulose, hemicellulose, pectin and glycoproteins. Even though the components of PCWs have been well studied, there is still limited understanding of the 3D architecture (Cosgrove 2001, 2014; Wang and Hong 2016). This lack of understanding is largely attributed to the complex nature of the interactions between cellulose and other PCW components. Since the first two high-resolution solid-state NMR studies of cellulose were published in 1980 (Atalla et al. 1980; Earl and VanderHart 1980), solid-state NMR spectroscopy has been an important tool in the study of the 3D architecture of PCWs. Solid-state NMR spectroscopy not only revealed the polymorphic structure of cellulose but also detailed the interactions between cellulose and other macromolecules in intact plant cell walls (Dick-Pérez et al. 2011; Earl and VanderHart 1981; Larsson et al. 1999; Newman and Hemmingson 1995; Wang and Hong 2016; Wang et al. 2016a).

Solid-state NMR spectroscopy of cellulose produces doublet δ^{13}C4 peaks that have been used to estimate the degree of crystallinity of cellulose as well as the number of glucan chains in elementary cellulose microfibrils (Kennedy et al. 2007; Newman et al. 1994, 1996; Park et al. 2009; Teeäär et al. 1987; Wang et al. 2015). Two δ^{13}C4 peaks, centered at $\sim$ 89 and $\sim$ 85 ppm, have been assigned to ordered (crystalline) and disordered (amorphous) regions, respectively (Atalla et al. 1980; Earl and VanderHart 1980). This assignment was based on the dominance of 89-ppm signals in highly crystalline cellulose and was tested by ball-milling microcrystalline cellulose sample which led to increased intensity of the 85 ppm peak and a simultaneous decrease in the intensity of the 89 ppm peak (Maciel et al. 1982). The two peaks have also been assigned as the signals from solvent-exposed and interior chains, respectively (Ha et al. 1998; Newman 1998). The intensity ratio between these two peaks gives information about the number of chains in the microfibril, which is consistent with the results obtained from diffraction methods and absorption spectroscopy, which collectively constrain the cross-sectional dimension of cellulose microfibrils (Fernandes et al. 2011). However, the molecular structures of cellulose responsible for the specific surface and interior C4 peaks have not been positively confirmed.

This study examines the role that structural factors could play in changing δ^{13}C4 values using Density Functional Theory (DFT) and structures produced via classical MD simulations. Suzuki et al. (2009) have applied DFT calculations on monosaccharide and disaccharide models in vacuum to demonstrate that ^{13}C4 NMR chemical shifts can be influenced by conformations of exocyclic groups at C6 (*tg*, *gt* and *gg*), glycosidic bond angles (Φ, Ψ) as well as the H atom at the γ-C OH position (C3). However, monosaccharide and disaccharide models differ greatly from a cellulose microfibril and as a result there were significant differences ($\sim$ 10 ppm) between the calculated and observed δ^{13}C values. For example, compared to the cellulose experimental δ^{13}C4 values of 79–93 ppm (Park et al. 2009), their calculated δ^{13}C4 were between $\sim$ 65 and $\sim$ 75 ppm. To improve the agreement between observation and calculation, in the work presented here, we utilized an Iβ cellulose model system containing 12 cellotetraose chains with three different conformations of the C6 exocyclic group (*tg*, *gt* and *gg*) as shown in Fig. 1 (Wang et al. 2016b; Watts et al. 2014). The atomic positions of these models had previously been energy-minimized using DFT under periodic boundary conditions (Kubicki et al. 2013). The cellulose model used here is merely a minimal structure that contains both interior (two) and surface (ten) cellulose chains and is of a size that is computationally practical for DFT calculations. It is not intended to suggest that a cellulose microfibril contains only twelve chains. In our previous work, by using Iβ (110) and Iβ (100) surface models, we demonstrated that H_2O molecules affected the calculated δ^{13}C4 values of glucose residues with *tg* conformation (Kubicki et al. 2014). In this paper, using both DFT and classical structures, we investigated how the following four factors affect C4 NMR chemical shifts: conformations of exocyclic groups at C6 (*tg*, *gt* and *gg*), H_2O molecules H-bonded to the surface, glycosidic bond angles (Φ, Ψ) and the

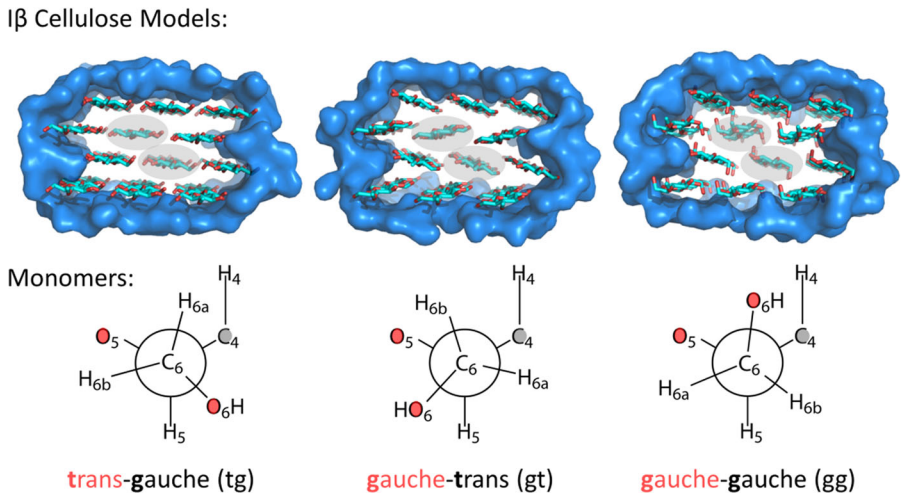

Fig. 1 Solvated cellulose Iβ models with three different conformations of the C6 exocyclic group (*tg*, *gt* and *gg*, respectively). Each model was produced to be three chains wide, four layers high and four monomer units in length, and was solvated with explicit H_2O molecules. The middle two glucan units in the shaded regions represent the cellulose interior while all other glucan units are either surface or terminal. Only H_2O within 3 Å of the cellulose cluster (as shown in blue) were included in the following NMR shielding tensor calculations. Bottom: the *tg*, *gt* and *gg* conformers refer to the trans- and gauche states of the dihedral angle O5–C5–C6–O6 and C4–C5–C6–O6, O5 O6 were colored in red and C4 was colored in grey. (Color figure online)

position of the proton (HO3) of the OH group connected to the adjacent carbon C3. The effect of each factor on δ^{13}C4 was quantified using the computational protocol from our previous work (Kubicki et al. 2013).

Method

As shown in Fig. 1, cellulose Iβ models with three different conformations of the C6 exocyclic group (*tg*, *gt* and *gg*) were created based on X-ray and neutron diffraction structures of cellulose (Nishiyama et al. 2002). The atomic positions of these models have been previously energy minimized with periodic DFT-D2 calculations (Kubicki et al. 2013, 2014; Watts et al. 2014). As described previously, clusters were produced to be three chains wide, four layers high and four monomer units in length (Wang et al. 2016b), designated as the 4 × 3 × 4 cluster hereafter. This allows for four glucan monomers to have at least one other unit next to them in all three dimensions to represent the atomic environment within cellulose. The middle two glucan units in each chain were used to represent interior ^{13}C NMR chemical shifts. The O4 at the non-reducing end and C1 at the reducing end were terminated with $–CH_3$ and $–OCH_3$ groups, respectively, to satisfy the bonding of the terminal atoms.

Using the Impact module of Maestro (Schrödinger 2014), we solvated the cellulose clusters with TIP3P water (Jorgensen et al. 1983) in a 50 × 50 × 40 Å^3 box containing about 3000 H_2O molecules. Energy minimizations and molecular dynamics simulations were performed using the OPLS_2005 force field (Banks et al. 2005) keeping the atomic positions of cellulose molecules fixed. 1000 steps of conjugate gradient minimization were performed before 10 ps molecular dynamics simulations at 298 K with a 1 fs time step in the NVT ensemble. In addition to the 4 × 3 × 4 cellulose clusters, H_2O molecules were included in the NMR shielding tensor calculations. Only H_2O molecules within 3 Å of the cellulose clusters were included as it was found that H_2O molecules further than 3 Å from the clusters had negligible effects on the calculated δ^{13}C.

Larger models were impractical due to the total memory usage limit (256 GB) on the computing server. In order to test the sensitivity of the calculated NMR chemical to the size of the cellulose models, relatively smaller 3-layer cellulose models were generated, as shown in supplementary Fig. S1. NMR chemical shifts calculated from 3-layer and 4-layer

models are highly consistent to each other, as shown in supplementary Table S1, indicating that the size of our cellulose model (4 × 3 × 4 cellulose clusters) will not affect the quality of the cellulose ^{13}C NMR predictions. Hence, 4 × 3 × 4 cellulose clusters were deemed suitable to study the effects of the aforementioned structural factors on the NMR chemical shifts of cellulose. However, comparing to native cellulose microfibrils from primary cell walls, there are still many other factors that could potentially influence ^{13}C NMR that this current cellulose model (4 × 3 × 4 cellulose clusters) cannot account for, such as cellulose microfibril bundling, and interactions with other matrix polymers.

Rotating glycosidic bonds and torsion angle χ3 (C2–C3–O3–HO3)

To assess the effect of different glycosidic bond angles (Φ: O5′–C1′–O–C4, Ψ: C1′–O–C4–C5) on the ^{13}C NMR chemical shifts, a rigid potential energy surface (PES) scan was performed in Φ/Ψ space on a 7 × 7 grid with a step size of 10°, where $-123.2 \leq \Phi \leq -63.2$ and $-183.2 \leq \Psi \leq -123.2$, using M06-2X/6-31G(d) method (Rassolov et al. 2001; Zhao and Truhlar 2008) in Gaussian 09 (Frisch et al. 2010), a reliable method that has been applied constantly to obtain reasonable molecular structures for organic molecules (Fradon et al. 2017; Khansari et al. 2017; Zhao and Truhlar 2008; Zhou et al. 2017). Forty-nine cellulose tetramer chain conformations with different Φ/Ψ angles were generated for each C6 conformers (*gg*: C4–C5–C6–O6 = 57.2°; *gt*: C4–C5–C6–O6 = 178.1°; *tg*: C4–C5–C6–O6 = 285.7°). Those conformations were then subjected to NMR shielding tensor calculations.

To assess the effect of the position of HO3 on δ^{13}C4, a rigid PES scan was also performed on torsion angle χ3 (C2–C3–O3–HO3) of a cellulose tetramer chain with three different conformations of the C6 exocyclic group (*gg*: C4–C5–C6–O6 = 57.2°; *gt*: C4–C5–C6–O6 = 178.1°; *tg*: C4–C5–C6–O6 = 285.7°) from models being energy minimized previously with periodic DFT-D2 calculations. Torsion angle χ3 was rotated through 360° with a step of 10° using the M06-2X/6-31G(d) method in Gaussian 09. Cellulose tetramer chain conformations generated with different torsion angle χ3 values were then subjected to NMR shielding tensor calculations.

NMR shielding tensor calculations

NMR shielding tensors were calculated as described previously (Kubicki et al. 2013). This protocol has been shown to achieve an RMS error of better than 3 ppm for cellulose Iβ and Iα (Kubicki et al. 2013; Toukach and Ananikov 2013; Wang et al. 2016b). The modified Perdue–Wang exchange–correlation functional mPW1PW91 (Adamo and Barone 1998) with the 6-31G(d) basis set (Rassolov et al. 2001) and gauge-independent atomic orbitals (GIAO) (Bühl et al. 1999; Cheeseman et al. 1996; Karadakov 2006; Lodewyk et al. 2011; Schreckenbach and Ziegler 1995; Wiitala et al. 2006; Wolinski et al. 1990) method in Gaussian 09 were used. Chemical shifts were calculated using the multi-reference method. Methanol was the secondary standard to calculate the ^{13}C chemical shift, because it produces δ^{13}C in better agreement with experiment (Kubicki et al. 2013, 2014; Sarotti and Pellegrinet 2009; Watts et al. 2011, 2014). An empirical correction of 49.5 ppm (Gottlieb et al. 1997) was used for the difference between the δ^{13}C in methanol and TMS commonly used as an experimental ^{13}C NMR standard (Sarotti and Pellegrinet 2009).

$$\delta 13C_{calc,MeOH} + \delta 13C_{exp,MeOH}$$

This gives an isotropic chemical shielding of 193.0 ppm. To compute the δ^{13}C for any C nucleus *i* in cellulose, we used:

$$\delta 13C_i = 193.0 \text{ ppm} - \delta 13C_i$$

Results and Discussion

Different conformations of exocyclic groups at C6 (*tg*, *gt* and *gg*)

The interior cellulose chains were used to assess the effects that different conformations of exocyclic groups at C6 (*tg*, *gt* and *gg* conformation) had on the δ^{13}C in cellulose Iβ. Average calculated chemical shifts for each conformation of exocyclic groups at C6 are presented in Table 1. The largest effect was observed on the δ^{13}C4 (Table 1), where, compared to the *tg* conformation, *gt* and *gg* conformations shifted δ^{13}C4 upfield by ~ 1.4, and ~ 6.9 ppm, respectively. Given the moderate standard deviations, the

C4 peaks from *tg* and *gt* conformations would be indistinguishable within computational error whereas those from *gg* are outside expected model uncertainties. Consistent with previous results, the *gt* and *gg* conformations of C6 shifted the δ^{13}C6 by relatively large values upfield compared to the *tg* conformation (3 and 3.8 ppm, respectively). This is in good agreement with the CP-MAS NMR experimental finding by Horri et al. (1983) that *gg*, *gt* and *gt* conformations have incremental δ^{13}C6 values of 60–62.6, 62.5–64.5, 65.5–66.5 ppm, respectively. Considering the relatively small standard deviations (0.6 and 0.8 ppm, respectively), these signals are distinguishable from the *tg* conformer, yet it would be difficult to discern the *gt* from the *gg* signal (as observed experimentally where these two peaks are merged).

δ^{13}C1 for the *gt* and *gg* conformations were upfield shifted by $\sim$ 2 ppm compared to the *tg* conformation, however, the standard deviations were of a higher magnitude and therefore, it was not possible to distinguish between δ^{13}C1 with different C6 conformations. This could explain why the peak separation at the C1 region of ^{13}C NMR spectrum only happens within a small chemical shift range of 2 ppm (Jorgensen et al. 1983; Wang et al. 2016b). Similarly, the ^{13}C2 and ^{13}C5 chemical shifts were shifted by $\sim$ 2 ppm for *gt* and *gg* conformations, compared to the *tg* conformation, though downfield. Despite the standard deviations being reduced compared to the ^{13}C1 chemical shifts, it would be difficult to distinguish the peaks resulting from the different C6 conformations, and also from each other. Interestingly, the changing C6 conformations had a negligible effect on the ^{13}C3 chemical shifts, and these peaks would also merge with the ^{13}C2 and ^{13}C5 chemical shifts in an experimental spectrum.

Effects of H_2O H-bonding on the surface

Two sets of NMR calculations were conducted on each 4 × 3 × 4 clusters with three different conformations of the C6 exocyclic group (*tg*, *gt* and *gg*) to investigate the effect of changing C6 conformation for surface chains, and of H_2O H-bonding. One set of NMR calculation was conducted with H_2O molecules to mimic the cellulose microfibril in contact with water while the other set was conducted without any solvent molecules (in vacuum/gas state), to represent the cellulose microfibril in a dried state. In order to compare how these two conditions would affect ^{13}sC NMR chemical shifts (sC: C on the surface), we averaged the calculated chemical shifts at surface chains for each conformation of exocyclic groups at C6, as shown in supplementary Tables S2 and S3. We found that surface chains in a vacuum environment/dried state had downfield shifted δ^{13}sC4 (by $\sim$ 1–2 ppm), compared to interior chains. On the contrary, H_2O molecules cause an upfield shift (1 ± 1 ppm) in all ^{13}sC NMR chemical shifts except for δ^{13}sC4. For different C6 conformations δ^{13}sC4 values could be shifted either upfield or downfield depending on hydration (Table 2). We emphasize that the standard deviations in these averages are significant which means that the individual δ^{13}sC4 values could differ by 3–4 ppm from the δ^{13}sC4 values (e.g., *tg*(s) − *tg*(i) 1.5 ± 1.7 = 3.2 ppm). Consequently, dehydration of cellulose could mimic *tg* to *gt* rotations as far as the δ^{13}sC4 is concerned.

Focusing on the surface chains, the two adjacent surface C4 atoms have similar chemical environment (Oehme et al. 2015), however the C4–H4 group of adjacent glucose units point in opposite directions (Fig. 2). One points towards the solvent environment (designated as $C4_{H4\text{-}out}$), whereas the other points

Table 1 Calculated average δ^{13}C and standard deviations for interior cellulose (ppm). Differences from the *tg* conformation are listed as "*gt–tg*" and "*gg–tg*"

	C1	C2	C3	C4	C5	C6
δ^{13}C (*tg*)	104.0 ± 1.2	69.6 ± 0.1	72.2 ± 0.5	85.7 ± 0.5	70.9 ± 0.9	64.3 ± 0.1
δ^{13}C (*gt*)	102.1 ± 3.8	72.1 ± 1.5	72.0 ± 0.1	84.2 ± 1.1	71.8 ± 0.9	61.3 ± 0.7
δ^{13}C (*gg*)	101.9 ± 1.2	72.1 ± 0.9	71.7 ± 1.1	78.8 ± 1.1	72.7 ± 1.3	60.6 ± 0.9
δ^{13}C (*gt*)–δ^{13}C (*tg*)	− 1.9 ± 4.8	2.5 ± 1.5	− 0.2 ± 0.5	− 1.4 ± 1.6	1.0 ± 1.8	− 3.0 ± 0.6
δ^{13}C (*gg*)–δ^{13}C (*tg*)	− 2.2 ± 2.4	2.4 ± 1.0	− 0.5 ± 1.5	− 6.9 ± 1.6	1.9 ± 2.2	− 3.8 ± 0.8

Table 2 Effect of water or vacuum/dried state on the calculated δ^{13}C4 of glucose units on the surface (ppm)

		With water		Vacuum/dried state		Difference[b]
		δ^{13}sC4	$\Delta\delta^{13}$sC4[a]	δ^{13}sC4	$\Delta\delta^{13}$sC4	δ^{13}sC4
tg	H4-in	86.6 ± 1.6	0.9 ± 1.6	86.5 ± 1.2	0.8 ± 1.3	0.1
	H4-out	85.1 ± 1.4	− 0.6 ± 1.3	87.9 ± 1.8	2.2 ± 1.9	**− 2.8**
gt	H4-in	84.4 ± 2.3	− 0.1 ± 1.9	84.1 ± 2.8	− 0.2 ± 2.2	0.3
	H4-out	82.9 ± 1.3	− 1.3 ± 1.9	86.7 ± 2.2	2.5 ± 2.6	**− 3.8**
gg	H4-in	79.7 ± 1.4	0.9 ± 1.4	78.7 ± 1.3	− 0.1 ± 1.1	1.0
	H4-out	76.9 ± 1.4	− 2.0 ± 1.3	79.5 ± 1.4	0.7 ± 1.2	**− 2.6**

[a]$\Delta\delta^{13}$sC4 = *tg/gt/gg* at surface − *tg/gt/gg* at interior

[b]Difference = $\Delta\delta^{13}$sC4 with water − $\Delta\delta^{13}$sC4 at dried state. The H4-out residues showing significant chemical shift perturbation by water are highlighted in bold

away from the solvent environment to the interior cellulose microfibril (designated as $C4_{H4\text{-}in}$). We found that hydration had relative large effects on $\delta^{13}sC4_{H4\text{-}out}$, yet negligible effects on $\delta^{13}sC4_{H4\text{-}in}$. Water molecules upfield shifted $\delta^{13}sC4_{H4\text{-}out}$ of *gg* and *gt* conformers by ~ 2 and ~ 1.3 ppm, respectively. On the contrary, $\delta^{13}sC4_{H4\text{-}in}$ values of *gg* and *gt* conformers were either downfield shifted by ~ 0.9 ppm or upfield shifted by only ~ 0.1 ppm respectively. A vacuum environment had the opposite effects on ^{13}sC NMR chemical shifts of $C4_{H4\text{-}out}$ moving them downfield, whereas $C4_{H4\text{-}in}$, was affected in a similar manner to water-solvated chains. Directly comparing the δ^{13}sC4 with or without water solvent (last column of Table 2), we found that H4-out residues demonstrated much more significant chemical shift perturbation than H4-in residues did. This indicates that two adjacent C4 on the surface have different chemical environment with the C4 having its H4 pointing into the interior behaving like an interior C4, and only every other glucose δ^{13}sC4 is effected by H-bonding to water.

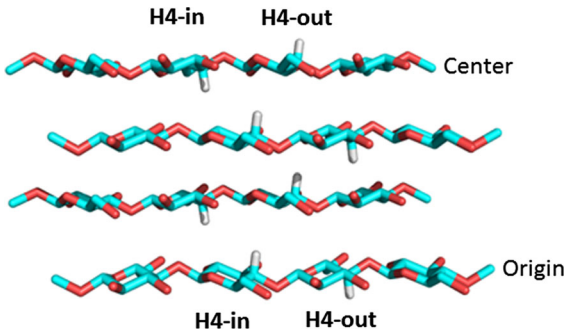

Fig. 2 C4–H4 groups of adjacent glucan units point to opposite directions in cellobiose-like units. C4–H4 pointing to the interior of the cluster is designated as H4-in, whereas C4–H4 pointing to the environment of the cluster is designated as H4-out

Averaging chemical shifts over all C atoms has the effect of ignoring key contributions that could be made by individual carbons. Previous work has shown that H-bonding from H_2O molecules to C4 had a significant effect (Kubicki et al. 2014). By examining individual glucose residues, we found that several δ^{13}C4 on the surface were downfield shifted by ~ 4–5 ppm due to the absence of H-bonding (H–O < 2.5 Å and O–H–O > 90°) (Kubicki et al. 2014) to H_2O molecules. This is comparable to the findings in Kubicki et al. (2014) and also explained the relative large standard deviations observed when the δ^{13}C4 are averaged.

Glycosidic bond angles (Φ Ψ)

Other factors that have been suggested to affect δ^{13}C4 are the Φ and Ψ dihedral angles (Φ: O5′–C1′–O–C4; Ψ: C1′–O–C4–C5; SI Fig. 1). The Φ and Ψ angles in the 4x3x4 clusters represent the glycosidic bond angles at the region of conformational minimum (Wang et al. 2016b), because the clusters were generated based on the X-ray and neutron diffraction structures of cellulose and energy minimized with periodic DFT-D2 calculations (Kubicki et al. 2013, 2014). However, it is unrealistic to think that all the Φ and Ψ angles in a biological sample would be at the conformational minimum. To obtain a more

realistic distribution of Φ and Ψ angles in a cellulose microfibril, the final structure from a MD simulation on an 18-chain Iβ cellulose microfibril model, published by Oehme et al. 2015, has also been utilized. To assess the dependence of δ^{13}C4 on the glycosidic dihedral angles (Ψ, Φ), a rigid potential energy surface scan was conducted on Φ and Ψ, where $-123.2° \leq \Phi \leq -63.2°$ and $-183.2° \leq \Psi \leq -123.2°$. The relative energies of the rigid PES scan and the distribution of Φ and Ψ angles obtained from MD simulations were plotted together in Fig. 3a. There was good agreement between allowed Φ/Ψ angles observed from MD simulations and the relative energies obtained from the rigid PES scan. As shown in Fig. 3a, almost all the allowed Φ/Ψ angles observed from the MD simulation were clustered into the low-energy zone, with relative potential energies no more than 20 kJ/mol above the minimum. The Φ/Ψ angles at the minimum were consistent with those angles in the 4 × 3 × 4 clusters as well as those angles in the X-ray crystal structure of cellulose Iβ, as shown in Fig. 3b.

The allowed Φ/Ψ angles observed from the MD simulation ($-163° \leq \Psi \leq -133°$ and $-113° \leq \Phi \leq -83°$) were plotted overlapped with the calculated relative δ^{13}C4 values, as shown in Fig. 3b, to estimate the effect of the allowed the Φ/Ψ angles on δ^{13}C4. Using the DFT minimized *tg* conformation as a reference, the allowed Φ/Ψ angles observed from MD simulations caused an upfield shift in δ^{13}C4 by up to 1.3 ppm in interior chains, and a more diverse shift of up to 5.7 ppm in surface chains.

In addition, when the C6 was in the *gt* or *gg* conformation, rotation about the glycosidic bond had a similar effect on δ^{13}C4. As shown in Supplementary Table S4 and S5, the allowed Φ/Ψ angles observed from MD simulations caused an upfield shift in δ^{13}C4 by up to 1.6 ppm (*gg*) and 1.4 ppm (*gt*) in interior chains, and a more diverse shift of up to 6.0 ppm (*gg*) and 6.4 ppm (*gt*) in surface chains.

δ^{13}C for the adjacent glucose units connected by the glycosidic bond of interest were also calculated, as shown in the supplementary materials (Supplementary Table S6). In addition to δ^{13}C4, only δ^{13}C1

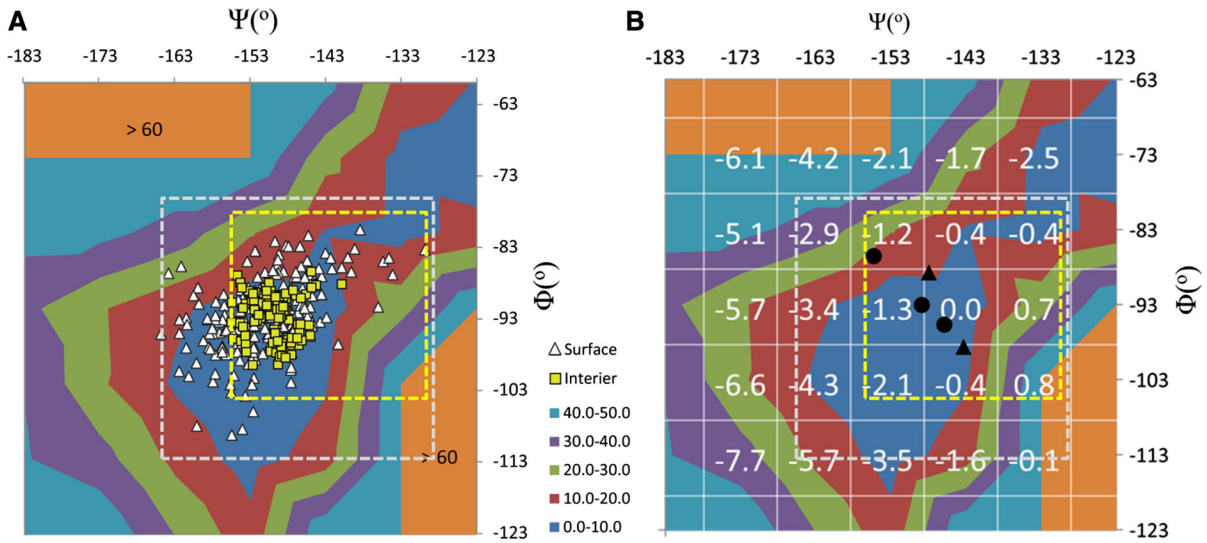

Fig. 3 **a** Overlapping the energy contour map of relative energies of cellotetramer (with C6 exocyclic groups at *tg* conformation) when rotating the glycosidic linkage dihedral angles Φ and Ψ with the observed dihedral angles Φ and Ψ from MD simulation, white triangles represent Φ/Ψ from surface chains in MD simulation, yellow squares represent Φ/Ψ from surface chains in MD simulation; **b** overlay of the contour map with the table of calculated relative δ^{13}C4 values for different dihedral angles Φ and Ψ. The regions where dihedral angles Φ and Ψ are observed in MD simulations are in grey dashed line square. The yellow dashed line square represented the crystalline conformational minimum (when $\Psi = -143° \pm 10°$ and $\Phi = -93° \pm 10°$). The three black dots represent the Φ/Ψ angles in the 4 × 3 × 4 clusters, −85°/−155°, −92°/−150° and −94°/−145° for *gg*, *gt* and *tg*, respectively. The two black triangles represent the Φ/Ψ angles from the X-ray structure of cellulose Iβ by Nishiyama et al. (2003). (Color figure online)

and δ^{13}C2 are appreciably influenced by the rotation about the glycosidic bond. As shown in Supplementary Table S6, using the DFT minimized *tg* conformation as the reference, δ^{13}C1 and δ^{13}C2 can be upfield shifted by up to ~ 3.8 ppm or downfield shifted by up to ~ 1.3 ppm. The rotation about the glycosidic bond had negligible effect on δ^{13}C6.

Applying DFT calculations on a cellobiose model, Suzuki et al. (2009) studied the dependence of δ^{13}C4 on the glycosidic Φ or Ψ angles separately. In their study, either Φ or Ψ was rotated in steps of 30° for a full 360° while keeping the other angle fixed. They found that in the region of the crystalline conformational minimum, δ^{13}C4 was dependent on both Φ/Ψ angles, but only δ^{13}C1 and δ^{13}C2 were dependent on Ψ. However, MD simulations demonstrated that both Φ and Ψ angles have the potential to rotate in a cellulose microfibril (Oehme et al. 2015). In this study, together with the allowed Φ/Ψ angles values provided via MD simulations on the 18-chain cellulose microfibril models, our study provided more detailed information of the dependence ^{13}C4 NMR chemical shifts on both Φ/Ψ angles. The effect that rotation about the glycosidic bond had on δ^{13}C4 was independent of the conformation at C6 (*gt, gg, tg*). In the region of the crystalline conformational minimum (when $\Psi = -143° \pm 10°$ and $\Phi = -93° \pm 10°$), where 100% of the Φ/Ψ angles for interior chains and ~ 60% of them for surface chains in MD simulations were sampled, δ^{13}C4 exhibit limited changes due to the limited variation of Φ/Ψ angles, with at most an upfield shift of ~ 2 ppm, consistent with our previous study (Kubicki et al. 2013). δ^{13}C4 were more sensitive to changes of the Φ/Ψ angles sampled by surface chains in MD simulations; the chemical shifts associated with these angles are upfield shifted by up to ~ 6 ppm.

Effect of adjacent HO3 group

The position of the proton (HO3) of the OH group connected to C3 has also been proposed to influence the ^{13}C4 NMR chemical shift (Suzuki et al. 2009). In order to investigate the relationship between HO3 and the ^{13}C4 NMR chemical shift, a PES, the distance between H4 and HO3, and the ^{13}C4 NMR chemical shift were all calculated for each C6 conformation and are plotted with respect to the HO3–O3/C4–H4 dihedral angle. From the PES, for all C6 conformations there is a global minimum when the HO3–O3/C4–H4 torsion angle is around 100°, which corresponds to a strong inter-residue H-bond forming between O3 and O5 (O5 of the adjacent glucose unit) (Fig. 4, conformation B). Inter-residue H-bond between O3 and O5 has been reported for both Iα and Iβ allomorphs, thus is common to native cellulose (Nishiyama et al. 2002, 2003). All the HO3 protons in the DFT energy minimized 4x3x4 clusters were also found to have the similar position as shown in the conformation B. Additionally, O3 can form a relative weak intra-residue H-bond with O2, which corresponds to a local minimum, when the HO3–O3/C4–H4 torsion angle was around 260° (Fig. 4). However, this minimum is not found for the *gg* conformation. As shown in supplementary Fig. S3, the *gg* conformations at C6 causes HO2 to be re-positioned, so the H-bond between O3 and O2 does not form.

^{13}C4 NMR chemical shifts were found to be influenced by the distance between H4 and HO3 (Fig. 4). As the distance between H4 and HO3 increased, δ^{13}C4 decreased, except when the HO3–O3/C4–H4 torsion angle was between 60° and 120°. Here, the δ^{13}C4 plot formed a plateau at around 88, 87 and 80 ppm for *tg*, *gt* and *gt* conformations, respectively, even though the distance between H4 and HO3 increased from about 2.5 to 3.1 Å. This was probably due to strong inter-residue H-bonding between O3–HO3 and O5′ (Fig. 4). When the distance between H4 and HO3 was at a maximum (~ 3.6 Å) with the torsion angle of HO3–O3/C4–H4 at ~ 203°, δ^{13}C4 reached a minimum, upfield shifted by ~ 2 ppm from the plateau. When the distance between H4 and HO3 was at a minimum (~ 2.1 Å) with the torsion angle of HO3–O3/C4–H4 at ~ 200°, δ^{13}C4 reached a maximum, downfield shifted by ~ 3 ppm from the plateau. A similar relationship between δ^{13}C1′ and the torsion angle O22–HO22/C12–H12 was also observed when rotating χ2 (C12C22O22HO22), as shown in supplementary Fig. S4.

Applying DFT calculations on a single glucose (with C6 at *gt* conformation) model Suzuki et al. (2009) found that ^{13}C4 NMR chemical shift could be influenced by the position of the H (HO3) of the OH group connected to the adjacent carbon C3. They explained this qualitatively as resulting from the γ_H-gauche effect and intra-residue H-bonds. They found that δ^{13}C4 was higher (75.1 and 77.2 ppm) when HO3 was at *gauche* position (when torsion angle of C2–C3–O3–HO3 was at 60° or 180°) compared to the δ^{13}C4 value (70.3 ppm) when HO3 was in a *trans* position

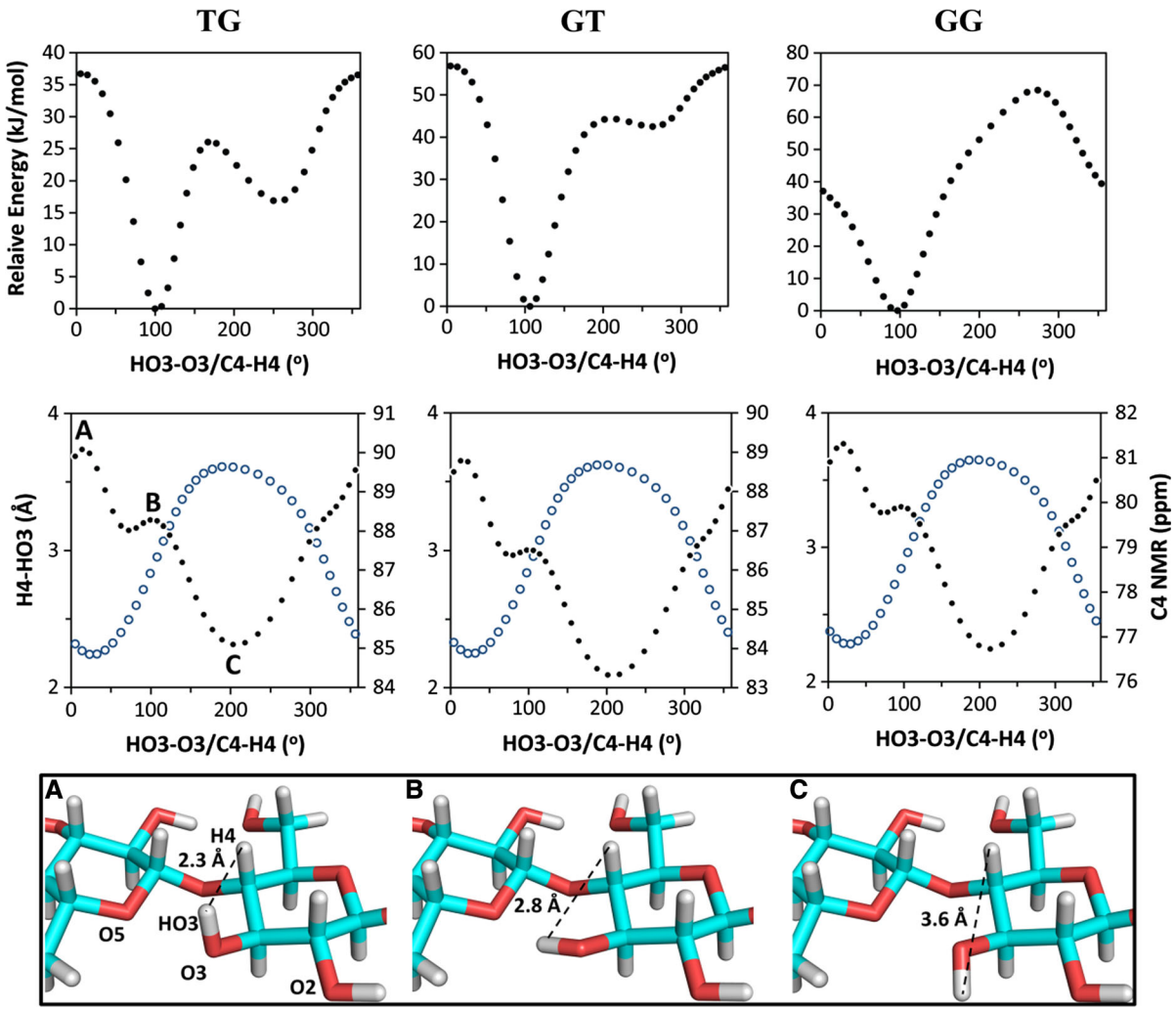

Fig. 4 Top row, relative potential energies of cellotetramers with respect to different torsion angle HO3–O3/C4–H4 when the exocyclic group at C6 taking *tg*, *gt* and *gg* conformations, respectively; Middle row, distances between H4 and HO3 (shown as circle, primary y-axis) and C4 NMR chemical shifts (shown as black dots, secondary y-axis) in relation to torsion angle HO3–O3/C4–H4.; Bottom row, representative structures of cellulose tetramer of *tg* conformation at the max δ^{13}C4 (conformation A), plateau/energy minimum (conformation B), and min δ^{13}C4 (conformation C)

(when the torsion angle of C2–C3–O3–HO3 was at 300°). Consistently, we found that δ^{13}C4 was higher ($\sim$ 89 and $\sim$ 88 ppm) when HO3 was in the *gauche* position (C2–C3–O3–HO3 = 60° or 180°), whereas when HO3 was at *trans* position (C2–C3–O3–HO3 = 300°), δ^{13}C4 was $\sim$ 85 ppm. However, the *gauche* or *trans* positions cannot be correlated precisely to the maximum or minimum δ^{13}C4 (when torsion angle of C2–C3–O3–HO3 was at $\sim$ 83° or $\sim$ 282°, respectively), which suggested that this γ_H-gauche effect provided by Suzuki and co-authors cannot fully account for the effect of HO3 position on δ^{13}C4.

In this study, we found that ^{13}C4 NMR chemical shift had an inverse relationship with the distance between H4 and HO3. The δ^{13}C4 reached a maximum when the distance between H4 and HO3 was shortest and a minimum when furthest apart. Also, the inter-residue H-bond between O3–HO3 and O52 was shown to affect the ^{13}C4 NMR chemical shift, which was not identified in the previous study due to the small size of the model. Our calculated δ^{13}C4 values were in good agreement with the experiment values (79–93 ppm)

(Park et al. 2009), which varied from 77 to 90 ppm. Due to the small size of the model from the previous work, their calculated δ^{13}C4 varied from 70 to 75 ppm, ~ 10 ppm lower than the experiment values.

Implications for interpreting observed solid-state ^{13}C NMR spectra of native cellulose in intact cell walls

As shown in Fig. 5, our calculated ^{13}C NMR chemical shifts have a reasonably good agreement with the observed ssNMR spectra of native cellulose inside the intact and native *Arabidopsis* primary cell wall (Wang and Hong 2016). Since the δ^{13}C4 value is the most significant observable for the same C atom within the cellulose structure, our analysis was focused on changes in the δ^{13}C4 value.

As shown in Fig. 6, considering the effects of different conformation of exocyclic groups at C6, water and vacuum environments on ^{13}C NMR chemical shifts, our calculated δ^{13}C4 were separated into two 'peaks', centered at ~ 79 and ~ 86 ppm, respectively. One 'peak' at upfield (~ 79 ppm) was dominated by *gg* conformers, whereas the other one at downfield (~ 86 ppm) was dominated by *tg* and *gt* conformers. Although the effect of H_2O molecules H-bonding was to shift the *gt* and *tg* conformers on the surface upfield, our calculations indicate that these upfield shifts (*gt*: − 0.6 ± 1.9 ppm, *tg*: 0.1 ± 1.6 ppm) were not large enough to explain the 'gap' in C4 doublet peak (~ 5.5 ppm). In addition to different conformations at C6 and H_2O molecules at the surface, δ^{13}C4 were shown to be affected by rotation about the glycosidic bond, and the position of HO3 (the proton of –OH group connected to the adjacent C3). Variation in dihedral angles about the glycosidic bond always caused an upfield shift in the δ^{13}C4. Combining DFT calculations and structures from classical MD simulations, we found that δ^{13}C4 were relatively insensitive (varied by up to ~ 2 ppm) to changes in the Φ/Ψ angles of interior cellulose chains, due to their small variation in the region of crystalline conformational minimum (Ψ = − 143 ± 10° and Φ = − 93 ± 10°) as sampled by MD. In comparison, changes of Φ/Ψ angles of surface cellulose chains could upfield shift δ^{13}C4 by up to around 4.3 ppm. There was an inverse relationship between δ^{13}C4 and the distance between H4 and HO3. When the distance between H4 and HO3 was at a maximum (~ 3.6 Å), δ^{13}C4 reached a minimum (~ 2 ppm upfield shift) while when at a minimum (~ 2.1 Å), δ^{13}C4 reached a maximum, (~ 3 ppm downfield shift). Interestingly, the inter-residue H-bonds between O3–HO3 and O5 or O2 were able to stabilize ^{13}C4 NMR chemical shift, even with the H4–HO3 distance increasing. Therefore, our study indicated that the C4 peak separation was due to a combination of the above four factors, the different conformation at C6, water/gas environment, Φ and Ψ angles, and the position of HO3. However, different conformations of the exocyclic groups at C6 have the greatest influence on δ^{13}C4 peak separation. The other three factors have secondary effects that increase the spread of the calculated C4 interior and surface peaks.

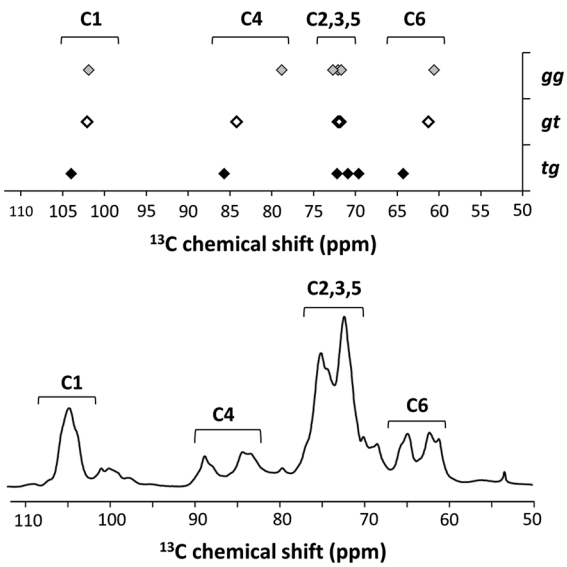

Fig. 5 Different conformations of the exocyclic groups at C6 have the greatest influence on δ13C. **a** Calculated average δ13C1-6 for *gg gt* and *tg* conformations by using the three models shown in Fig. 1; **b** 1D 13C cross polarization (CP) solid-state NMR spectrum of *Arabidopsis* primary cell wall measured on an 800 MHz spectrometer (Wang et al. 2016b). The cellulose-dominant peaks are labeled in the spectrum

This study was an attempt to interpret solid-state NMR spectra from a structural point of view. The iC4 peak (~ 89 ppm) was found to be dominated by the *tg* conformation, consistent with the previous finding from Wang et al. 2016a, b using a non-solvated cellulose model, though the *gt* conformation may also contribute to iC4 peak. For the sC4 peak (~ 85 ppm), two possible substructures could be contributing to the presence of this peak. It is either dominated by the *gt*

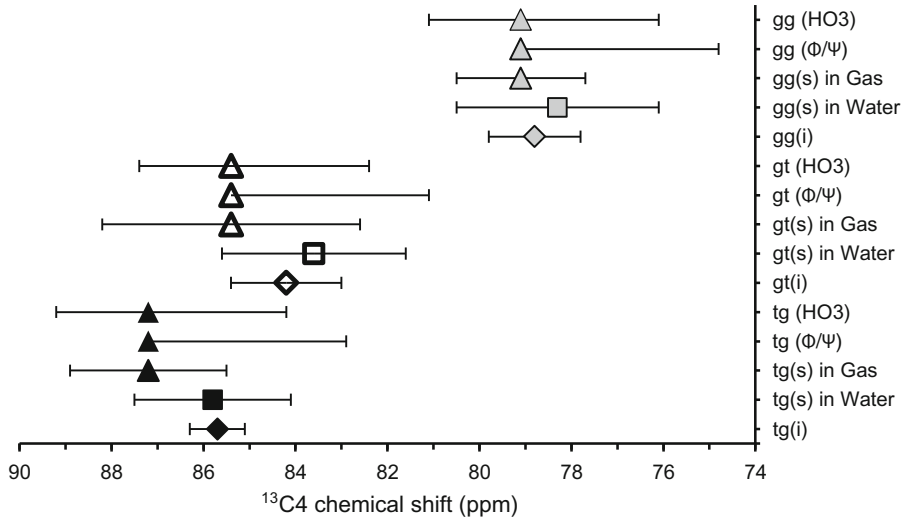

Fig. 6 Summary of the effects of different conformation of exocyclic groups at C6 [*tg*(i), *gt*(i) and *gg*(i)], solvent environment (water or gas/vacuum), glycosidic bond angles (Φ/Ψ), and position of HO3 atoms on δ^{13}C4. (i) represents the signals from interior cellulose whereas (s) represents signals from glucose on the surface of cellulose microfibril model. The horizontal error bars are the standard error except for effect of Φ/Ψ and HO3. The horizontal error bars in the effect of Φ/Ψ represented that changes of Φ/Ψ angles of surface cellulose chains could upfield shift δ^{13}C4 by 5.7 (*tg*), 6.0 (*gt*) and 6.4(*gg*) ppm. The horizontal error bars in the effect of HO3 represented the 3 ppm upfield shift or 2 ppm downfield shift due to the distance changing between H4 and HO3

conformation, as shown in Fig. 6, when it is further upfield shifted due to rotation about the glycosidic bond and the position of HO3, or it could be dominated by the *gg* conformation. The *gg* C4 chemical shift was centered at ∼ 79 ppm, which is out of the NMR C4 chemical shift range of 89–84 ppm. Our method cannot totally exclude the possibility that part of sC4 peak is dominated by *gg* C4, because the protocol we applied here has the RMS error of ∼ 3 ppm for cellulose Iβ and Iα (Kubicki et al. 2013; Toukach and Ananikov 2013). However, based on these calculations and analysis, we believe that the *gg* conformation is the least probable. This may not change the current predominant interpretation of the surface and interior nature of cellulose signals, however it is possible that a portion of cellulose may violate the surface-interior assignment. Therefore interior and surface percentages and crystallinity determined using the doublet δ^{13}C4 peaks may have limited accuracy. Our results still suggest that there is a link between the two peaks and that they can be classified as crystalline or amorphous as it would be expected that amorphous chains would have *gg* or *gt* conformation and crystalline will be *tg*. However, the calculations do suggest that not all amorphous chains will be represented by the upfield peak (∼ 85 ppm), and part of the signals from amorphous chains could reside in the downfield peak (∼ 89 ppm).

In addition to δ^{13}C4, we also found that δ^{13}C6 values were sensitive to the first two factors, the conformations at C6 and the H_2O molecules on the surface. As shown in Fig. 7, the calculated δ^{13}C6 were also separated into two 'peaks', centered at ∼ 61 and ∼ 64 ppm, respectively. The 'upfield peak' was dominated by *gg* and *gt* conformers, whereas the 'downfield peak' was dominated by *tg* conformers. The calculated results are in good agreement with the observed C6 peaks (centered at ∼ 62 and ∼ 65 ppm) in solid-state NMR spectra. This confirmed that the percentage of residues with *gt* and *gg* conformations can be estimated by calculating the size of the upfield C6 peak, whereas the percentage of residues with *tg* conformations can be estimated by the size of the downfield C6 peak (Horii et al. 1983; Oehme et al. 2015). In addition, microfibril bundling and intermolecular interactions with matrix polysaccharides, two factors crucial to wall mechanics, may also perturb the NMR chemical shifts of cellulose, thus are of high interest for future studies (Cosgrove 2016a, b).

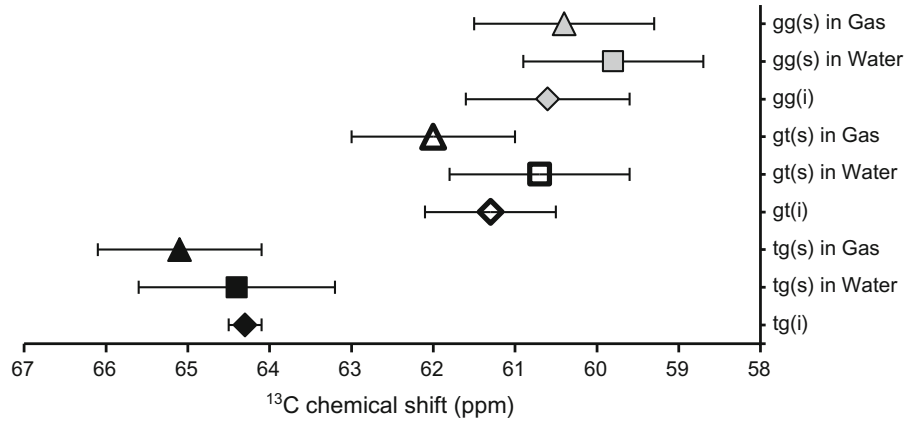

Fig. 7 Summary of the effects of different conformation of exocyclic groups at C6 [tg(i), gt(i) and gg(i)], solvent environment (water or gas/vacuum) on δ^{13}C6. (i) represents the signals from interior cellulose whereas (s) represents signals from glucose on the surface of cellulose microfibril model. The horizontal error bars are the standard error

Conclusion

In this paper, we have studied the structural factors that influence ^{13}C NMR chemical shifts in cellulose using DFT methods. We found that different conformations of the exocyclic groups at C6 (*gg*, *gt* and *tg* conformations) have the greatest influence on δ^{13}C4 peak separation, while other structural factors, such as H_2O molecules H-bonded on the surface of the microfibril, glycosidic bond angles (Φ, Ψ) and the distances between H4 and HO3 atoms, have secondary effects that increase the spread of the calculated C4 interior and surface peaks. We concluded that iC4 peak ($\sim$ 89 ppm) was dominated by the *tg* conformation, while sC4 ($\sim$ 85 ppm) peak was dominated by either *gg* or *gt* conformations. Hence, even though the conventional assignment of two C4 peaks observed by ^{13}C NMR to surface and interior regions may not be accurate; it is still possible that there is a link between the two peaks and that they can be classified as interior/crystalline or surface/amorphous regions.

Acknowledgments This work is supported by the Center for Lignocellulose Structure and Formation, an Energy Frontier Research Center funded by the U.S. Department of Energy, Office of Science, Basic Energy Sciences under Award # DE-SC0001090. Portions of this research were conducted with Advanced Cyber Infrastructure computational resources provided by the Institute for Cyber Science at The Pennsylvania State University (http://ics.psu.edu). This research also used resources of NERSC, supported by the Office of Science of DOE under Contract No. DE-AC02-05CH11231. This work was completed while DPO was at IBM Research Australia.

References

Adamo C, Barone V (1998) Exchange functionals with improved long-range behavior and adiabatic connection methods without adjustable parameters: the mPW and mPW1PW models. J Chem Phys 108:664–675

Atalla RH, Gast J, Sindorf D, Bartuska V, Maciel G (1980) Carbon-13 NMR spectra of cellulose polymorphs. J Am Chem Soc 102:3249–3251

Banks JL et al (2005) Integrated modeling program, applied chemical theory (IMPACT). J Comput Chem 26:1752–1780

Bühl M, Kaupp M, Malkina OL, Malkin VG (1999) The DFT route to NMR chemical shifts. J Comput Chem 20:91–105

Cheeseman JR, Trucks GW, Keith TA, Frisch MJ (1996) A comparison of models for calculating Nuclear Magnetic Resonance shielding tensors. J Chem Phys 104:5497–5509

Cosgrove DJ (2001) Wall structure and wall loosening. A look backwards and forwards. Plant Physiol 125:131–134

Cosgrove DJ (2014) Re-constructing our models of cellulose and primary cell wall assembly. Curr Opin Plant Biol 22:122–131

Cosgrove DJ (2016a) Catalysts of plant cell wall loosening. F1000Research 5:1

Cosgrove DJ (2016b) Plant cell wall extensibility: connecting plant cell growth with cell wall structure, mechanics, and the action of wall-modifying enzymes. J Exp Bot 67:463–476

Dick-Pérez M, Zhang Y, Hayes J, Salazar A, Zabotina OA, Hong M (2011) Structure and interactions of plant cell-wall polysaccharides by two-and three-dimensional magic-angle-spinning solid-state NMR. Biochemistry 50:989–1000

Duchesne LC, Larson D (1989) Cellulose and the evolution of plant life. Bioscience 39:238–241

Earl WL, VanderHart DL (1980) High resolution, magic angle sampling spinning Carbon-13 NMR of solid cellulose I. J Am Chem Soc 102:3251–3252

Earl WL, VanderHart DL (1981) Observations by high-resolution Carbon-13 Nuclear Magnetic Resonance of cellulose I related to morphology and crystal structure. Macromolecules 14:570–574

Fernandes AN et al (2011) Nanostructure of cellulose microfibrils in spruce wood. Proc Natl Acad Sci 108: E1195–E1203

Fradon A, Cloutet E, Hadziioannou G, Brochon C, Castet F (2017) Optical properties of donor–acceptor conjugated copolymers: a computational study. Chem Phys Lett 678:9–16

Frisch M et al (2010) Gaussian 09, revision B. 01. Gaussian, Inc, Wallingford

Gottlieb HE, Kotlyar V, Nudelman A (1997) NMR chemical shifts of common laboratory solvents as trace impurities. J Organ Chem 62:7512–7515

Ha MA et al (1998) Fine structure in cellulose microfibrils: NMR evidence from onion and quince. Plant J 16:183–190

Horii F, Hirai A, Kitamaru R (1983) Solid-state ^{13}C NMR study of conformations of oligosaccharides and cellulose. Polym Bull 10:357–361

Jorgensen WL, Chandrasekhar J, Madura JD, Impey RW, Klein ML (1983) Comparison of simple potential functions for simulating liquid water. J Chem Phys 79:926–935

Karadakov PB (2006) Ab initio calculation of NMR shielding constants. In: Webb GA (ed) Modern magnetic resonance. Springer, Berlin, pp 63–70

Kennedy CJ, Cameron GJ, Šturcová A, Apperley DC, Altaner C, Wess TJ, Jarvis MC (2007) Microfibril diameter in celery collenchyma cellulose: X-ray scattering and NMR evidence. Cellulose 14:235–246

Khansari ME, Mirchi A, Pramanik A, Johnson CR, Leszczynski J, Hossain MA (2017) Remarkable hexafunctional anion receptor with operational urea-based inner cleft and thiourea-based outer cleft: novel design with high-efficiency for sulfate binding. Sci Rep 7:6032

Kubicki JD, Mohamed MN-A, Watts HD (2013) Quantum mechanical modeling of the structures, energetics and spectral properties of Iα and Iβ cellulose. Cellulose 20:9–23

Kubicki JD, Watts HD, Zhao Z, Zhong L (2014) Quantum mechanical calculations on cellulose–water interactions: structures, energetics, vibrational frequencies and NMR chemical shifts for surfaces of Iα and Iβ cellulose. Cellulose 21:909–926

Larsson PT, Hult E-L, Wickholm K, Pettersson E, Iversen T (1999) CP/MAS ^{13}C-NMR spectroscopy applied to structure and interaction studies on cellulose I. Solid State Nucl Magn Reson 15:31–40

Lodewyk MW, Siebert MR, Tantillo DJ (2011) Computational prediction of ^{1}H and ^{13}C chemical shifts: a useful tool for natural product, mechanistic, and synthetic organic chemistry. Chem Rev 112:1839–1862

Maciel GE, Kolodziejski WL, Bertran MS, Dale BE (1982) Carbon-13 NMR and order in cellulose. Macromolecules 15:686–687

Newman RH (1998) Evidence for assignment of 13C NMR signals to cellulose crystallite surfaces in wood, pulp and isolated celluloses. Holzforschung 52:157–159

Newman RH, Hemmingson JA (1995) Carbon-13 NMR distinction between categories of molecular order and disorder in cellulose. Cellulose 2:95–110

Newman RH, Ha M-A, Melton LD (1994) Solid-state ^{13}C NMR investigation of molecular ordering in the cellulose of apple cell walls. J Agric Food Chem 42:1402–1406

Newman RH, Davies LM, Harris PJ (1996) Solid-state ^{13}C Nuclear Magnetic Resonance characterization of cellulose in the cell walls of *Arabidopsis thaliana* leaves. Plant Physiol 111:475–485

Nishiyama Y, Langan P, Chanzy H (2002) Crystal structure and hydrogen-bonding system in cellulose Iβ from synchrotron X-ray and neutron fiber diffraction. J Am Chem Soc 124:9074–9082

Nishiyama Y, Sugiyama J, Chanzy H, Langan P (2003) Crystal structure and hydrogen bonding system in cellulose Iα from synchrotron X-ray and neutron fiber diffraction. J Am Chem Soc 125:14300–14306. https://doi.org/10.1021/ja037055w

Oehme DP, Downton MT, Doblin MS, Wagner J, Gidley MJ, Bacic A (2015) Unique aspects of the structure and dynamics of elementary Iβ cellulose microfibrils revealed by computational simulations. Plant Physiol 168:3–17

Park S, Johnson DK, Ishizawa CI, Parilla PA, Davis MF (2009) Measuring the crystallinity index of cellulose by solid state ^{13}C Nuclear Magnetic Resonance. Cellulose 16:641–647

Rassolov VA, Ratner MA, Pople JA, Redfern PC, Curtiss LA (2001) 6–31G* basis set for third-row atoms. J Comput Chem 22:976–984

Sarotti AM, Pellegrinet SC (2009) A multi-standard approach for GIAO ^{13}C NMR calculations. J Organ Chem 74: 7254–7260

Schrödinger L (2014) Schrödinger Release 2014-1: Maestro, version 9.7. New York, NY

Schreckenbach G, Ziegler T (1995) Calculation of NMR shielding tensors using gauge-including atomic orbitals and modern density functional theory. J Phys Chem 99:606–611

Suzuki S, Horii F, Kurosu H (2009) Theoretical investigations of ^{13}C chemical shifts in glucose, cellobiose, and native cellulose by quantum chemistry calculations. J Mol Struct 921:219–226

Teeäär R, Serimaa R, Paakkarl T (1987) Crystallinity of cellulose, as determined by CP/MAS NMR and XRD methods. Polym Bull 17:231–237

Toukach FV, Ananikov VP (2013) Recent advances in computational predictions of NMR parameters for the structure elucidation of carbohydrates: methods and limitations. Chem Soc Rev 42:8376–8415

Wang T, Hong M (2016) Solid-state NMR investigations of cellulose structure and interactions with matrix polysaccharides in plant primary cell walls. J Exp Bot 67:503–514

Wang T, Park YB, Daniel JC, Hong M (2015) Cellulose-Pectin spatial contacts are inherent to never-dried *Arabidopsis Thaliana* primary cell walls: evidence from solid-state NMR. Plant physiology 168:871–884

Wang T, Phyo P, Hong M (2016a) Multidimensional solid-state NMR spectroscopy of plant cell walls. Solid State Nucl Magn Reson 78:56–63

Wang T, Yang H, Kubicki JD, Hong M (2016b) Cellulose structural polymorphism in plant primary cell walls investigated by high-field 2D solid-state NMR spectroscopy and Density Functional Theory calculations. Biomacromolecules 17:2210–2222

Watts HD, Mohamed MNA, Kubicki JD (2011) Comparison of multistandard and TMS-standard calculated NMR shifts for coniferyl alcohol and application of the multistandard method to lignin dimers. J Phys Chem B 115:1958–1970

Watts HD, Mohamed MNA, Kubicki JD (2014) A DFT study of vibrational frequencies and ^{13}C NMR chemical shifts of model cellulosic fragments as a function of size. Cellulose 21:53–70

Wiitala KW, Hoye TR, Cramer CJ (2006) Hybrid density functional methods empirically optimized for the computation of ^{13}C and ^{1}H chemical shifts in chloroform solution. J Chem Theory Comput 2:1085–1092

Wolinski K, Hinton JF, Pulay P (1990) Efficient implementation of the gauge-independent atomic orbital method for NMR chemical shift calculations. J Am Chem Soc 112: 8251–8260

Zhao Y, Truhlar DG (2008) The M06 suite of density functionals for main group thermochemistry, thermochemical kinetics, noncovalent interactions, excited states, and transition elements: two new functionals and systematic testing of four M06-class functionals and 12 other functionals. Theoret Chem Acc 120:215–241

Zhou C-C, Hawthorne MF, Houk KN, Jiménez-Osés G (2017) Multiple mechanisms for the thermal decomposition of metallaisoxazolin-5-ones from computational investigations. J Organ Chem 82:8438–8443